SYNTHETIC BIOLOGY

Electrogenetic cellular insulin release for real-time glycemic control in type 1 diabetic mice

Krzysztof Krawczyk[1]*, Shuai Xue[1,2], Peter Buchmann[1], Ghislaine Charpin-El-Hamri[3], Pratik Saxena[1], Marie-Didiée Hussherr[1], Jiawei Shao[2,4], Haifeng Ye[2], Mingqi Xie[1,4], Martin Fussenegger[1,5]†

Sophisticated devices for remote-controlled medical interventions require an electrogenetic interface that uses digital electronic input to directly program cellular behavior. We present a cofactor-free bioelectronic interface that directly links wireless-powered electrical stimulation of human cells to either synthetic promoter–driven transgene expression or rapid secretion of constitutively expressed protein therapeutics from vesicular stores. Electrogenetic control was achieved by coupling ectopic expression of the L-type voltage-gated channel $Ca_V1.2$ and the inwardly rectifying potassium channel $K_{ir}2.1$ to the desired output through endogenous calcium signaling. Focusing on type 1 diabetes, we engineered electrosensitive human β cells ($_{Electro}$β cells). Wireless electrical stimulation of $_{Electro}$β cells inside a custom-built bioelectronic device provided real-time control of vesicular insulin release; insulin levels peaked within 10 minutes. When subcutaneously implanted, this electrotriggered vesicular release system restored normoglycemia in type 1 diabetic mice.

Precise control of dosage is essential for the success of any drug-based therapy (*1*–*4*). However, taking pills or administering biopharmaceuticals at regular intervals based on body weight, as is standard medical practice, is far from being precise and does not reflect the dynamics required for sophisticated metabolic interventions (*1*–*4*). Cell-based therapies capitalizing on implanted encapsulated designer cells engineered to fine-tune in situ production and systemic delivery of protein therapeutics in response to chemical and physical cues have shown promising results in proof-of-concept studies (*5*, *6*). Because chemical control input is often limited, traceless physical cues such as light (optogenetics) (*7*–*10*) or heat [transmitted by magnetic fields (magnetogenetics) or radio waves (radiogenetics) (*11*–*14*)] are attractive for achieving rapid remote control of therapeutic transgene expression because they avoid the side effects of chemical trigger compounds (*15*, *16*) as well as the challenges they may present with respect to bioavailability or pharmacodynamics (*17*–*20*). However, available physically triggered gene switches may require a high energy input (*6*, *7*, *9*), often involve complex chemical or inorganic cofactors (*12*, *21*), and may require fine-tuning of the transcription of the therapeutic transgenes, which slows down the overall response dynamics (*5*, *6*, *9*, *12*, *22*). Thus, direct cofactor-free wireless electrical stimulation of engineered cells to control vesicular secretion of protein therapeutics in a robust, adjustable, and repeatable manner would offer substantial advantages for medical applications by enabling direct communication between electronic devices and designer cells.

Although cellular metabolism and human-made electronics share similar operating principles in terms of input sensing, information processing, and output production, the core information transfer and processing functions of living and electronic systems are different, which limits their interoperability. Humans use ion gradients across insulated membranes to simultaneously process slow analog chemical reactions and communicate information in multicellular systems through soluble or gaseous molecular signals. In contrast, electronic systems use multicore central processing units to control the flow of electrons through insulated metal wires with gigahertz frequency and communicate information across networks via wired or wireless connections. Thus, direct electrical stimulation of gene expression or vesicular secretion requires a bioelectronic interface that manages electrical conduction between electrodes and electrosensitive designer cells, as well as conversion of electronic information via depolarization to protein production and release.

The first attempts to create an electrogenetic interface were reported more than a decade ago (*23*, *24*), but that interface was neither direct nor usable under physiological conditions. More recently, a SoxR-based redox system that can control gene expression in *Escherichia coli* was reported (*25*), but this was also indirect and was too toxic for in vivo application. Thus, despite decades of expertise in converting trigger-inducible bacterial and fungal repressor-operator interactions into synthetic mammalian gene switches, simple translation of bacterial electrogenetics into a mammalian cellular context has been unsuccessful because of the cytotoxicity, limited bioavailability, and poor clinical compatibility of electrosensitive redox compounds (*23*).

With the advent of optogenetics, it became possible to use illumination to control target gene expression remotely, and thus to indirectly link electrical stimulation via a light source with cellular transcription control (*6*, *10*). This enabled glycemic control of experimental type 2 diabetes by controlling an optogenetic biomedical implant with a smartphone to upload instructions for designer cells to produce and systemically deliver a therapeutic dose of an insulinogenic peptide (*6*). However, the optogenetic device requires a considerable amount of energy to operate the light source (*6*, *10*). The power efficiency associated with direct electrical stimulation is a major reason why clinically licensed pacemakers can be battery-powered for a lifespan of at least 15 years (*26*). Other major challenges to the clinical application of optogenetic technology include illumination-based cytotoxicity (*27*), the use of bacterial components (*6*, *10*, *18*–*20*), and the need for sophisticated chemical or inorganic cofactors that have side effects (*28*–*30*), poor bioavailability, or short half-lives in vivo (*31*). Other traceless physical control technologies based on electro-induced heat transmission, such as magneto- and radiogenetics, share the same challenges (*12*, *21*, *32*, *33*).

Diabetes is a common, chronic condition, and so is an attractive target for individualized precision treatment. Regulation of blood glucose levels is a closed-loop homeostatic process. Glucose-stimulated insulin release by pancreatic β cells involves uptake and metabolism of glucose, adenosine triphosphate–mediated closure of potassium channels, depolarization of the plasma membrane, and opening of the voltage-gated calcium channels, which results in an intracellular Ca^{2+} surge and concurrent rapid release of insulin from intracellular storage vesicles (*34*). For intervention in this process, we aimed to design a bioelectronic interface consisting of an implantable platform that combines electronics and electrosensitive designer cells that can release insulin on demand. The implant would incorporate a cell chamber containing semipermeable membranes that permit nutrient supply and product delivery via fibrous connective tissue, while protecting the designer cells from cellular host responses (*35*, *36*) and securely containing them for safety reasons (*37*). To address this need, we describe here a direct cofactor-free electrogenetic interface

[1]Department of Biosystems Science and Engineering, ETH Zurich, CH-4058 Basel, Switzerland. [2]Shanghai Key Laboratory of Regulatory Biology, Institute of Biomedical Sciences and School of Life Sciences, East China Normal University, Shanghai 200241, People's Republic of China. [3]Département Génie Biologique, Institut Universitaire de Technologie Lyon 1, F-69622 Villeurbanne Cedex, France. [4]Key Laboratory of Growth Regulation and Transformation Research of Zheijang Province, School of Life Sciences, Westlake University, Hangzhou, People's Republic of China. [5]Faculty of Science, University of Basel, CH-4058 Basel, Switzerland.
*Present address: Novartis Pharma AG, CH-4002 Basel, Switzerland.
†Corresponding author. Email: fussenegger@bsse.ethz.ch

to trigger vesicular secretion of insulin by using electrical stimulation to modulate the membrane polarization of human β cells engineered for ectopic expression of calcium and potassium channels ($_{Electro}$β cells). Furthermore, to validate our approach, we incorporated these electrosensitive designer cells into a bioelectronics implant and evaluated its performance in a mouse model of type 1 diabetes.

Membrane depolarization–based transcriptional control in mammalian cells

L-type voltage-gated calcium channels consist of α_1, α_2, δ, and β subunits and are essential for the functioning of cardiomyocytes, neurons, and endocrine cells (*38*). These channels open upon membrane depolarization, and the resulting calcium influx regulates muscle contraction, vesicular secretion of hormones, and NFAT (nuclear factor of activated T cells)–driven induction of target genes (*39*).

To design a mammalian transcription-control circuit responsive to membrane depolarization, we cotransfected human embryonic kidney (HEK) 293T cells with one of the three L-type voltage-gated calcium channels—$Ca_V1.2$, $Ca_V1.3_{42A}$, or $Ca_V1.3_{\Delta42}$—encoded by the common α_2/δ_1 ($pCa_V\alpha_2\delta_1$, P_{hCMV}-α_2/δ_1-pA) and β_3 ($pCa_V\beta_3$, P_{hCMV}-β_3-pA) subunits and the respective channel-forming subunits α_1C ($pCa_V1.2$, P_{hCMV}-α_1C-pA), α_1D_{42A} ($pCa_V1.3_{42A}$, P_{hCMV}-α_1D_{42A}-pA), or $\alpha_1D_{\Delta42}$ ($pCa_V1.3_{\Delta42}$, P_{hCMV}-$\alpha_1D_{\Delta42}$-pA), as well as the reporter plasmid pMX57 encoding the human placental secreted alkaline phosphatase (SEAP) driven by the P_{NFAT3} promoter (pMX57, P_{NFAT3}-SEAP-pA) (Fig. 1A). Depolarization of channel-transgenic HEK-293T cells with 40 mM KCl revealed that ectopic expression of $Ca_V1.2$ showed the highest depolarization-triggered SEAP induction (Fig. 1B).

Coexpression of the inwardly rectifying potassium channel $K_{ir}2.1$ ($pK_{ir}2.1$, P_{hCMV}-$K_{ir}2.1$-pA), which has been reported to decrease the resting membrane potential of mammalian cells (*40*), substantially decreased basal SEAP expression and improved the overall induction profile of the depolarization-triggered $Ca_V1.2$-mediated transcription control device (Fig. 1C). Combinatorial analysis of the importance of $Ca_V1.2$'s individual components for overall depolarization-triggered transcription control revealed that the channel-forming α_1C subunit was essential, whereas α_2/δ_1 and β_3 were not, although their absence reduced the maximum SEAP expression (fig. S1). Therefore, we used cells expressing the full $Ca_V1.2$ with the α_1C, α_2/δ_1, and β_3 components as well as Kir2.1, referred to as $_{Electro}$HEK, in all follow-up experiments. Note that $_{Electro}$HEK cells are not activated by physiological ion concentrations, not even at life-threatening levels of KCl [6.5 mM (*27*)] or at $CaCl_2$ levels representing a medical emergency [3.5 mM (*28*)] (fig. S2).

Design and characterization of a synthetic electrogenetic mammalian transcription-control device

To test whether transgene expression could be directly triggered by electrically stimulated membrane depolarization, we used voltage-controlled square unipolar pulses with alternate polarization to electrostimulate the $_{Electro}$HEK cells transfected with the P_{NFAT3}-driven SEAP expression vector (pMX57, P_{NFAT3}-SEAP-pA) (*41*–*43*) (Fig. 2A). Indeed, electric pulse stimulation triggered pMX57-transgenic $_{Electro}$HEK cells to produce high levels of SEAP (Fig. 2, B to D). The electrostimulated transgene expression could be fine-tuned by voltage (maximum SEAP induction at 50 V) (Fig. 2B) and could also be adjusted by altering the pulse length (maximum SEAP induction at 2 ms) (Fig. 2C).

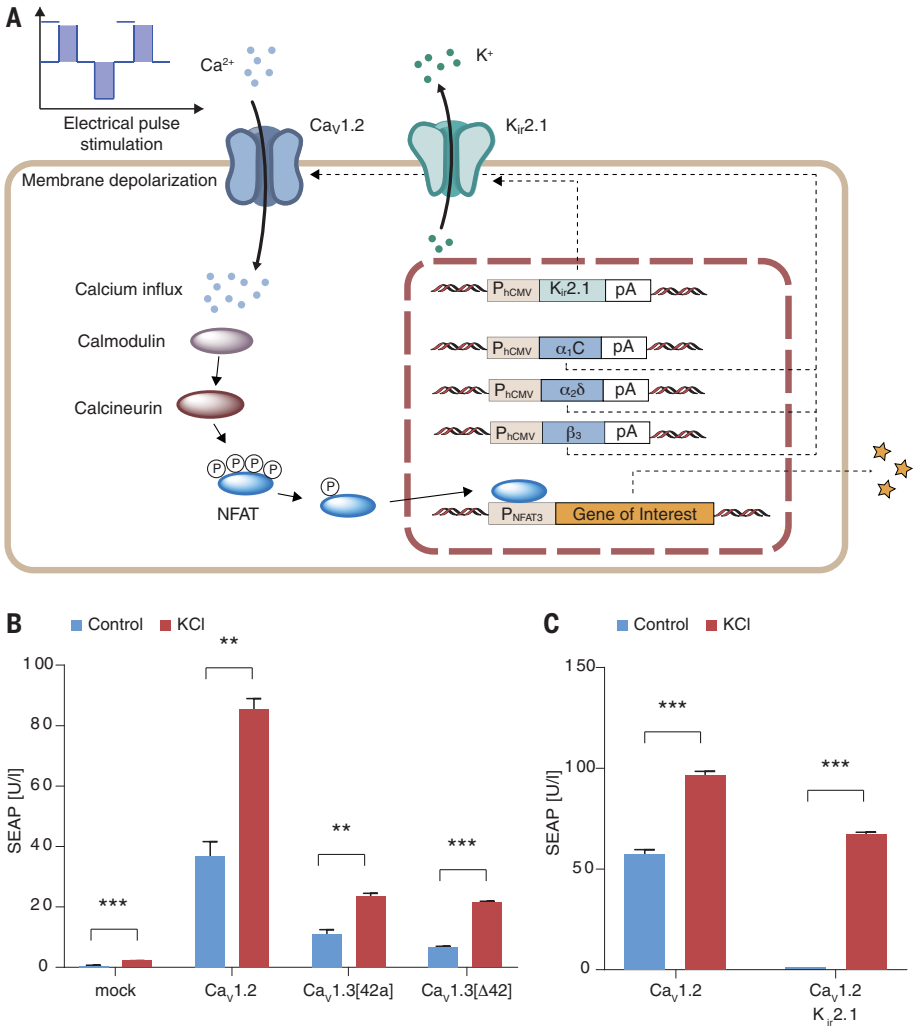

Fig. 1. Design of the electrogenetic circuit in mammalian cells. (**A**) Schematic representation of the electrogenetic circuit. The inwardly rectifying potassium channel lowers the resting membrane potential of HEK-293T cells, and electrical pulses depolarize the plasma membrane and open the L-type voltage-gated calcium channel. Calcium influx activates the calmodulin/calcineurin pathway, which leads to dephosphorylation of NFAT and its translocation to the nucleus, where it activates the NFAT-sensitive promoter and triggers transgene expression. (**B**) Comparative performance of three L-type voltage-gated calcium channels. Cells were cotransfected with P_{NFAT3}-driven SEAP reporter plasmid (pMX57), plasmids encoding α_2/δ_1 ($pCa_V\alpha_2\delta_1$, P_{hCMV}-α_2/δ_1-pA) and β_3 ($pCa_V\beta_3$, P_{hCMV}-β_3-pA), and one of the pore-forming subunits: α_1C ($pCa_V1.2$, P_{hCMV}-α_1C-pA), α_1D_{42A} ($pCa_V1.3_{42A}$, P_{hCMV}-α_1D_{42A}-pA), and $\alpha_1D_{\Delta42}$ ($pCa_V1.3_{\Delta42}$, P_{hCMV}-$\alpha_1D_{\Delta42}$-pA), to form $Ca_V1.2$, $Ca_V1.3_{42A}$, and $Ca_V1.3_{\Delta42}$, respectively. pcDNA3.1(+) was used as a mock plasmid. The cell membrane was depolarized with 40 mM potassium chloride (red bars); after 24 hours, SEAP was quantified in the supernatant. Blue bars show negative controls. (**C**) Coexpression of L-type voltage-gated calcium channel $Ca_V1.2$ and inwardly rectifying potassium channel $K_{ir}2.1$. Cells were cotransfected with $pCa_V1.2$ (P_{hCMV}-α_1C-pA), $pCa_V\alpha_2\delta_1$ (P_{hCMV}-α_2/δ_1-pA), $pCa_V\beta_3$ (P_{hCMV}-β_3-pA), pKK05 (P_{hCMV}-$K_{ir}2.1$-pA), and pMX57 (P_{NFAT3}-SEAP-pA) in the molar proportions 1:1:1:1:3. Cells were depolarized with 40 mM KCl for 24 hours (red bars) and SEAP was quantified in supernatant samples. Data are means ± SEM; $n = 3$. $^{**}P < 0.01$, $^{***}P < 0.001$ (versus control).

Full activation of the system was reached after 4 hours of stimulation (Fig. 2D). Electrostimulation efficiency did not depend on the pulsing frequency within the range of 0.5 to 10 Hz (Fig. 2E). The parameter set used for effective electrostimulation did not decrease cell viability (fig. S3, A to D). Additionally, $Ca_V1.2$-deficient HEK-293T cells were insensitive to electrostimulation (fig. S3E). Kinetic experiments revealed maximum SEAP expression 7 hours after the beginning of stimulation (fig. S4A) and confirmed the reversibility of the system (fig. S4B).

Design of the bioelectronic implant

Translation of electrostimulated gene expression into a clinical proof-of-concept bioelectronic implant required a more compact design for electrodes and electrostimulation. Simple miniaturization of the free-hanging electrodes used in the device described above did not provide efficient electrostimulation. Thus, we designed a custom-engineered cell culture insert containing electrodes on either side of a semipermeable membrane harboring a monolayer of electrosensitive $_{Electro}$HEK cells (Fig. 3A). Electrostimulation of pMX57 (P_{NFAT3}-SEAP-pA)–transfected $_{Electro}$HEK cells resulted in peak SEAP levels at 7.5 V (Fig. 3, B and C), which is one order of magnitude lower than that of the previous free-hanging electrode arrangement, and at shorter pulse length (Fig. 3, D and E); both factors are important for high power efficiency of any electrostimulation device.

To enable electrostimulated transgene expression by electrosensitive cells in vivo, we designed a wireless-powered bioelectronic implant. The custom-engineered cell culture insert equipped with the electrodes was clicked into a 3D-printed FDA-licensed polyamide casing (Fig. 4, A and B) containing a sealed electronic switchboard (figs. S5 and S6) that generated the square unipolar pulses for electrostimulation of the encapsulated $_{Electro}$HEK cells. The implant's electronic circuitry was inductively powered and controlled by an extracorporeal field generator that wirelessly communicated with the bioelectronic implant at the ISM (industrial, scientific, and medical) frequency of 13.56 MHz (Fig. 4B and figs. S7 and S8). The voltage of the square pulses generated by the implant was dependent on the distance to the center of the field generator (fig. S9). The electronic circuit was insensitive to temperatures between 25° and 50°C (table S1). A control run of the bioelectronic implant validated wireless-controlled electrostimulated SEAP expression of pMX57-transfected $_{Electro}$HEK cells (Fig. 4C). We confirmed that the bioelectronic implants are rated IPX7 waterproof (International Protection Marking, IEC standard 60529) and show no cell leakage in a 5-day in vitro experiment (table S2).

$_{Electro}$β cells provide electrostimulated vesicular secretion

Because $_{Electro}$HEK-based insulin production is transcription-based, it lacks the rapid release dynamics of vesicular secretion characteristic of native pancreatic β cells (*5*). To engineer mammalian cells for electrostimulated vesicular release of insulin (Fig. 5A), we derived a monoclonal population, INS_{Vesc}, from the pancreatic β cell line 1.1E7 (*44*) by selection for deficiency in glucose sensitivity (Fig. 6, E and F), but with retention of the vesicular insulin secretion machinery. Indeed, electron micrographs of $_{Electro}$β cells, an INS_{Vesc} variant stably transgenic for constitutive expression of $Ca_V1.2$ and $K_{ir}2.1$ channels (pKK66, $P_{hEF1\alpha}$-α_1C-P2A-K_{ir}2.1-pA; pMX251, $P_{hEF1\alpha}$-α_2/δ_1-P2A-β_3-pA) as well as Proinsulin-NanoLuc, a designer construct engineered to co-secrete insulin and the *Oplophorus gracilirostris* luciferase (NanoLuc) at an equimolar ratio in endocrine cell types (*45*) (Fig. 5A), revealed storage vesicles reminiscent of insulin-containing

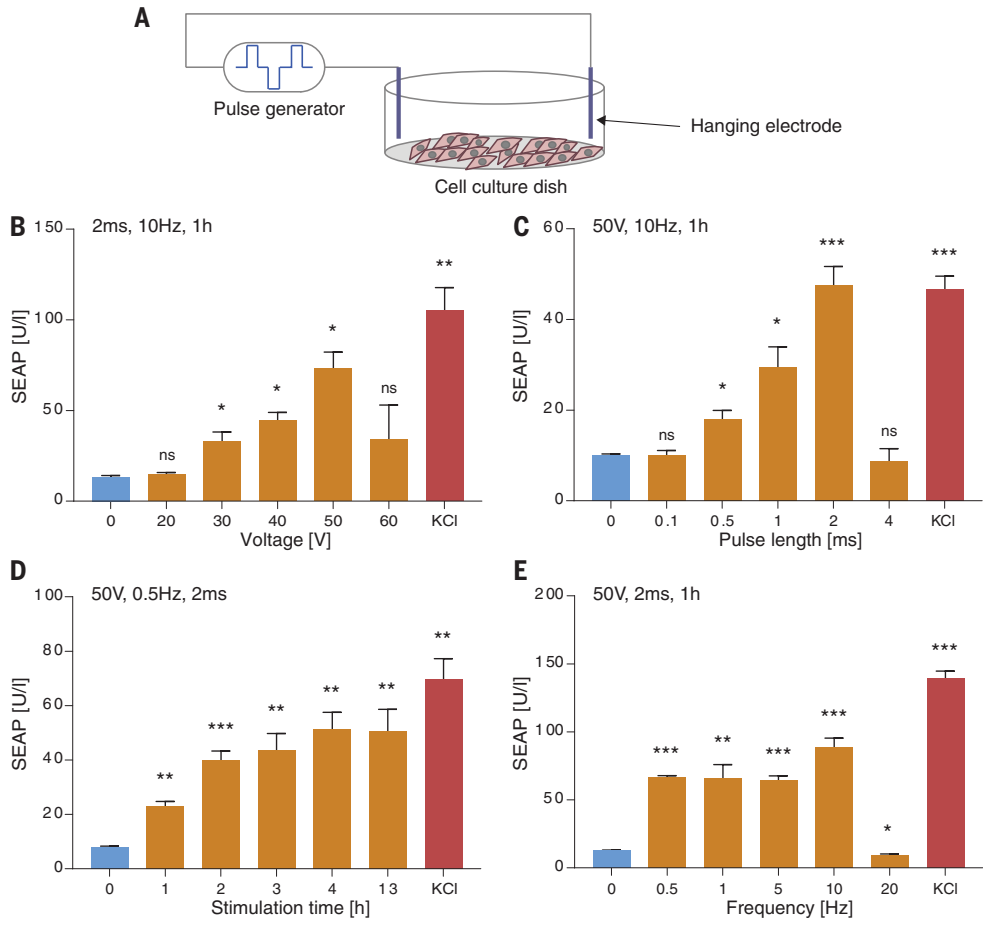

Fig. 2. Characterization of the electrogenetic circuit in vitro. (**A**) Schematic representation of electrical stimulation setup. Cells were stimulated with carbon hanging electrodes producing monopolar pulses with alternate polarization. (**B** to **E**) Cells were cotransfected with $pCa_V1.2$ (P_{hCMV}-α_1C-pA), $pCa_V\alpha_2\delta_1$ (P_{hCMV}-α_2/δ_1-pA), $pCa_V\beta_3$ (P_{hCMV}-β_3-pA), pKK05 (P_{hCMV}-K_{ir}2.1-pA), and pMX57 (P_{NFAT3}-SEAP-pA) in the molar proportions 1:1:1:1:3. SEAP assay was performed 24 hours after the beginning of the electrical stimulation procedure. Blue, orange, and red bars respectively denote unstimulated controls, electrically stimulated samples, and cells depolarized with 40 mM KCl. (B) Voltage dependence. Electrical stimulation was performed for 1 hour with 2-ms pulses at 10 Hz and the indicated voltage. (C) Pulse length effect. Electrical stimulation was performed for 1 hour at 10 Hz, 50 V, and the indicated pulse length. (D) Time course. Electrical stimulation was performed for the indicated period of time with 2-ms pulses at 0.5 Hz and 50 V. (E) Frequency effect. Electrical stimulation was performed for 1 hour with 2-ms pulses at 50 V and at the indicated frequency. Data are means ± SEM; $n = 3$. *$P < 0.05$, **$P < 0.01$, ***$P < 0.001$ (versus control); ns, not significant.

granules of human islet-derived β cells (Fig. 5, D and E). Additionally, $_{Electro}$β cells showed well-correlated vesicular insulin and NanoLuc secretion in response to KCl-mediated (Fig. 5, B and C) or electrostimulated (Fig. 6, A and B) membrane depolarization. The stability and functionality of the $_{Electro}$β cell line were confirmed over at least 30 passages during 3 months in continuous culture (fig. S10).

We profiled the depolarization-based insulin release dynamics by electrostimulating $_{Electro}$β cells and recording the corresponding NanoLuc-mediated luminescence in the culture supernatant (Fig. 6C). Peak NanoLuc levels were reached within 10 min after electrostimulation (Fig. 6C), whereas transcription-based insulin production and secretion by $_{Electro}$HEK, HEK-β (*5*), and $_{Opto}$HEK cells (*9*) required 8 hours (fig. S11). When repeatedly electrostimulated, $_{Electro}$β cells recovered full secretory capacity after 4 hours (Fig. 6D). Most important, $_{Electro}$β cells did not show any glucose-sensitive insulin production, which ensures exclusive electrostimulation control of vesicular insulin secretion without interference from blood glucose levels (Fig. 6, E and F). Overall, $_{Electro}$β cells showed electrostimulation parameters similar to those of $_{Electro}$HEK cells (fig. S12, A to D). To illustrate the broad applicability of our approach, we also demonstrated electrostimulated vesicular secretion of glucagon by pancreatic alpha cells, which secrete the insulin counterregulatory hormone glucagon by calcium-triggered vesicular release (*46*) (fig. S13); this is akin to β cell–mediated insulin secretion.

Wireless electrostimulated vesicular secretion of insulin provides rapid glycemic control in type 1 diabetic mice

Native pancreatic β cells release the insulin stored in granules via a process known as vesicular secretion (*34*). The immediate release of stored insulin improves the response dynamics and rapidly restores blood glucose homeostasis in response to postprandial excursions. So far, designer cell–based proof-of-concept strategies to treat experimental diabetes have focused on transcriptional control, which is considered too slow to cope with postprandial blood glucose surges (*5*, *6*, *12*, *14*, *21*). For example, previously reported HEK-β cells (*5*), which rely on transcriptional control and the classical secretory pathway for insulin release, require up to 24 hours to reach physiological blood insulin levels (fig. S14). Similar performance was observed for $_{Opto}$HEK cells (*9*). In contrast, when placed into the wireless-powered bioelectronic implant (Fig. 4), $_{Electro}$β cells could reestablish postprandial glucose metabolism in insulin-deficient type 1 diabetic mice after a brief electrostimulation without causing hypoglycemic excursions (Fig. 7A) and could rapidly decrease blood glucose levels to restore normoglycemia after electrostimulation (Fig. 7B). Notably, the results of glucose tolerance tests revealed comparable performance between $_{Electro}$β cells and human pancreatic islets, which are known to release insulin by vesicular secretion upon glucose sensing (fig. S7A). Fast vesicular secretion was also confirmed by blood luminescence quantification (*47*), which showed a peak signal just 1 hour after electrostimulation, returning to baseline after 2 hours (Fig. 7C). Glycemia could also be controlled over longer periods of time without any sign of hypoglycemia (Fig. 7D).

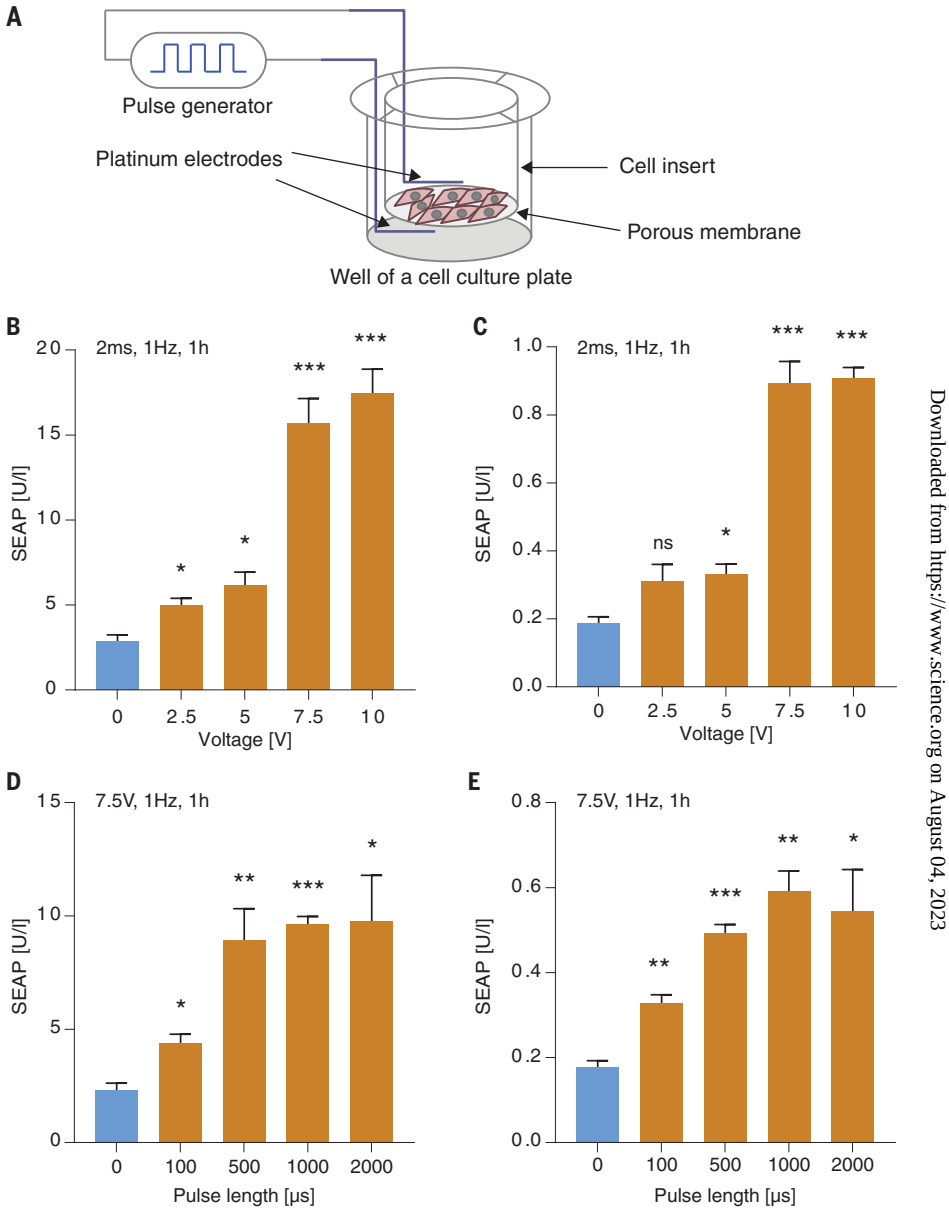

Fig. 3. Design and functionality of the bioelectronic implant in vitro. (**A**) Schematic representation of the stimulation setup in a cell culture insert. Two platinum electrodes (blue) were placed on opposite sides of the porous membrane covered with cells, and electrical pulse stimulation was applied. SEAP was quantified 24 hours after stimulation in the supernatants of the cell culture insert (above the membrane) and the well of the cell culture plate (below the membrane) to confirm that the secreted protein diffused across the membrane of the cell culture insert. (**B** and **C**) Voltage-dependent response of electrically stimulated pMX57-transfected $_{Electro}$HEK cells grown in a cell culture insert. Cells were stimulated with 2-ms pulses at 1 Hz for 1 hour (orange bars). SEAP was measured in supernatant samples from the cell culture insert (above the membrane) (B) and from the cell culture well (below the membrane) (C). Blue bars denote negative controls. (**D** and **E**) Pulse length dependence. Cells were stimulated with 7.5 V pulses at 1 Hz for 1 hour (orange bars). SEAP was measured from supernatant samples from above (D) and below the cell layer (E). Blue bars denote negative controls. Data are means ± SEM; $n = 3$. *$P < 0.05$, **$P < 0.01$, ***$P < 0.001$ (versus unstimulated control).

Biocompatibility and functional longevity of the bioelectronic implant

To validate the biocompatibility of the bioelectronic implants, we analyzed treated animals as well as explanted devices at 3 weeks after implantation, according to ISO 10993 (*48*), and we observed no material cytotoxicity, systemic kidney or liver toxicity, or alteration of hematologic profile or systemic immune responses; in addition, we saw no local immune-cell infiltration or substantial fibrotic tissue formation at the implant-tissue interface. There was no apparent indication of implant-related cytotoxicity (fig. S15) or systemic toxicity (table S3), and no apparent difference in hematologic profiles among cell-containing and cell-free bioelectronic implants and biocompatible control implants (table S4). Likewise, we found no marked difference in the well-vascularized fibrous capsule surrounding the implants (fig. S16) or in immune-cell infiltration (fig. S17 and table S5) among cell-containing, cell-free, and biocompatible control implants. Mice implanted with $_{\text{Electro}}\beta$ cell–containing bioelectronic devices showed no change of body weight relative to untreated animals; also, signs of irritation or inflammation, as well as serum levels of inflammatory cytokines, were similar to or lower than those of animals treated with cell-free or biocompatible reference implants (figs. S18 and S19). Visual inspection of explanted bioelectronic devices showed no decomposition and no apparent erosion (fig. S20).

In view of the need for clinical translation toward a lifestyle-compatible therapeutic product, we adapted the bioelectronic implant architecture to allow repetitive exchange of individual cell batches over time (fig. S20A). Sequential in situ "refilling" of the implanted bioelectronic device with fresh batches of $_{\text{Electro}}\beta$ cells without the need for surgical removal or replacement of the implant will reduce cost as well as implant-associated infections, while increasing patients' convenience and treatment longevity. Insulin levels of type 1 diabetic mice, which had the $_{\text{Electro}}\beta$ cells of their bioelectronic implants replaced once a week for a period of 3 weeks, were restored after remote-controlled electrostimulated insulin release by $_{\text{Electro}}\beta$ cells (fig. S20, B and C). Together, these results suggest that the bioelectronic implant successfully integrates the advantages of electronics-based (*49*) and cell-based counterparts (*5*) and represents a promising approach to diabetes treatment.

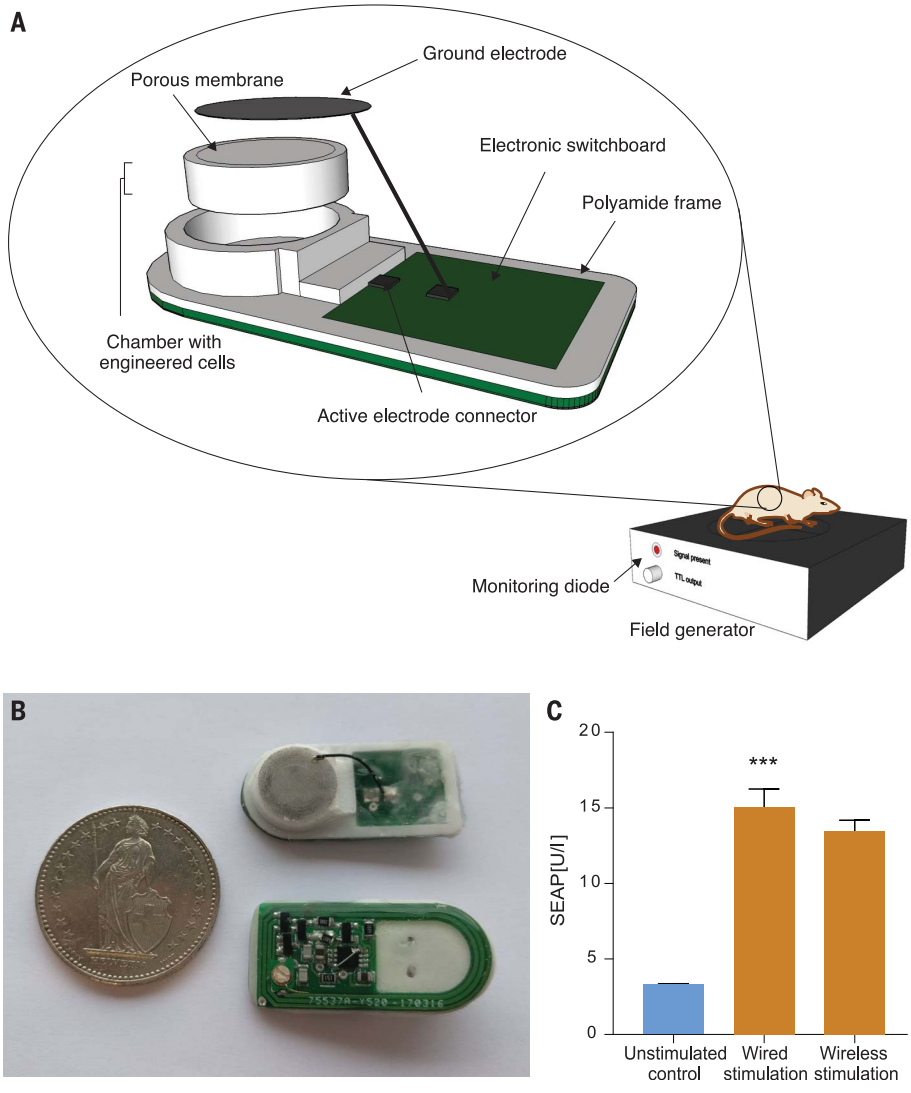

Fig. 4. Bioelectronic implant in vitro. (**A**) Three-dimensional model of a disassembled bioelectronic implant. A ring containing a porous membrane on one side can be assembled with a 3D-printed polyamide frame to form a cell chamber. The electronic switchboard is placed on the other side of the frame. The active platinum electrode (placed in the cell chamber; invisible in the model) is soldered to a connector on a switchboard. The ground electrode, made out of thin stainless steel mesh, is connected to the second connector on a switchboard. The bioelectronic implant can be placed subcutaneously on the dorsal side of the mouse, with the cell chamber facing down. The field generator provides wireless energy transmission. A red diode enables implant function monitoring. (**B**) Photograph of two bioelectronic implants with a coin (diameter 27.4 mm) for comparison. (**C**) Comparison of external generator–powered and implant-powered electrostimulation of pMX57-transfected $_{\text{Electro}}$HEK cells. SEAP was measured in supernatant samples from above the cell layer. Data are means ± SEM; $n = 3$. ***$P < 0.001$ (versus control).

Discussion

In this work, we have eliminated the need to use light as a converter between electronics and genetics, advancing optogenetics into electrogenetics by engineering a direct, cofactor-free electrogenetic interface that enables electronics to directly program gene expression as well as vesicular secretion in human cells. Furthermore, by incorporating electrogenetic designer cells ($_{\text{Electro}}\beta$) containing this interface into a bioelectronic implant, we have successfully implemented a proof-of-concept device providing rapid electrostimulated insulin release for the treatment of experimental type 1 diabetes. The overall slow response dynamics associated with transcription-based control systems (*5*, *6*, *9*, *10*, *12*, *15*, *16*, *18*–*21*) highlights the importance of vesicular secretion for the treatment of diabetes, which requires quick vesicular release of insulin to respond rapidly to postprandial blood glucose surges (*50*, *51*). Indeed, we found that wireless electrical stimulation of vesicular insulin release from our engineered $_{\text{Electro}}\beta$ cells encapsulated in a bioelectronic implant could attenuate postprandial hyperglycemia in type 1 diabetic mice with performance comparable to that of transplanted human pancreatic islets.

Taking account of the importance of economical manufacturing, we integrated all components of the bioelectronic implant into a 3D-printed polyamide casing. Although the

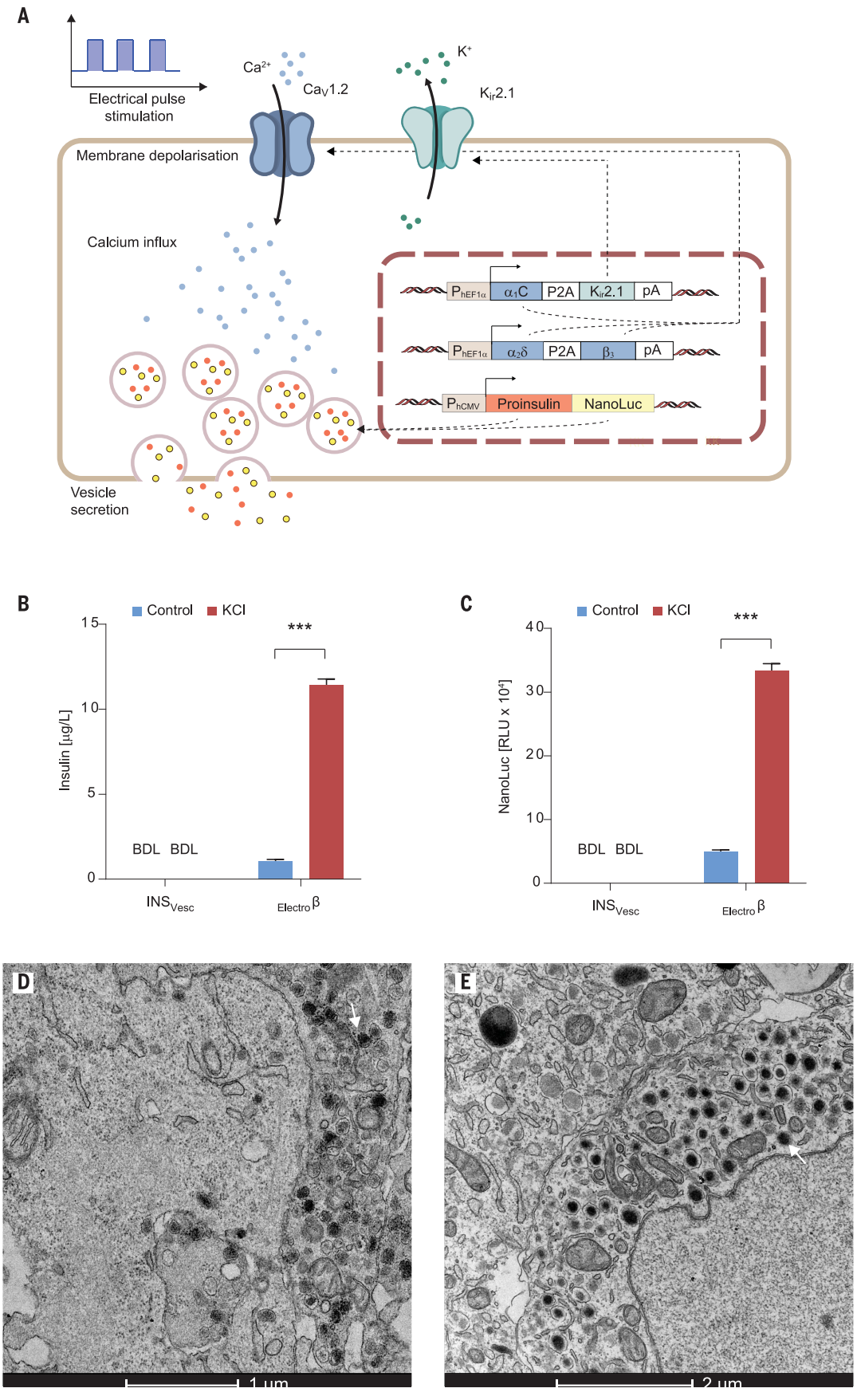

Fig. 5. Electrogenetic engineering of β cells. (**A**) Schematic representation of the electrically inducible insulin secretion pathway. The inwardly rectifying potassium channel $K_{ir}2.1$ lowers the resting membrane potential, which keeps the voltage-gated calcium channel $Ca_V1.2$ closed. Electrical pulse stimulation causes membrane depolarization, opening of $Ca_V1.2$, and calcium influx, which stimulates vesicle secretion. Vesicles are loaded with pre-produced insulin (red dots) and NanoLuc (yellow dots). (**B** and **C**) Comparison of insulin secretion by INS_{Vesc} and $_{Electro}\beta$ cells. Vesicle secretion was quantified by insulin-specific enzyme-linked immunosorbent assay (ELISA) (B) and luminescence (C) before (blue bars) and after depolarization with 40 mM KCl (red bars). BDL, below detection limit. Data are means ± SEM; $n = 3$. ***$P < 0.001$ (versus control). (**D**) Transmission electron microscopy (TEM) image of $_{Electro}\beta$ cells. White arrow indicates an insulin-containing vesicle. (**E**) TEM image of primary β cells from human pancreatic islets. White arrow indicates an insulin-containing vesicle.

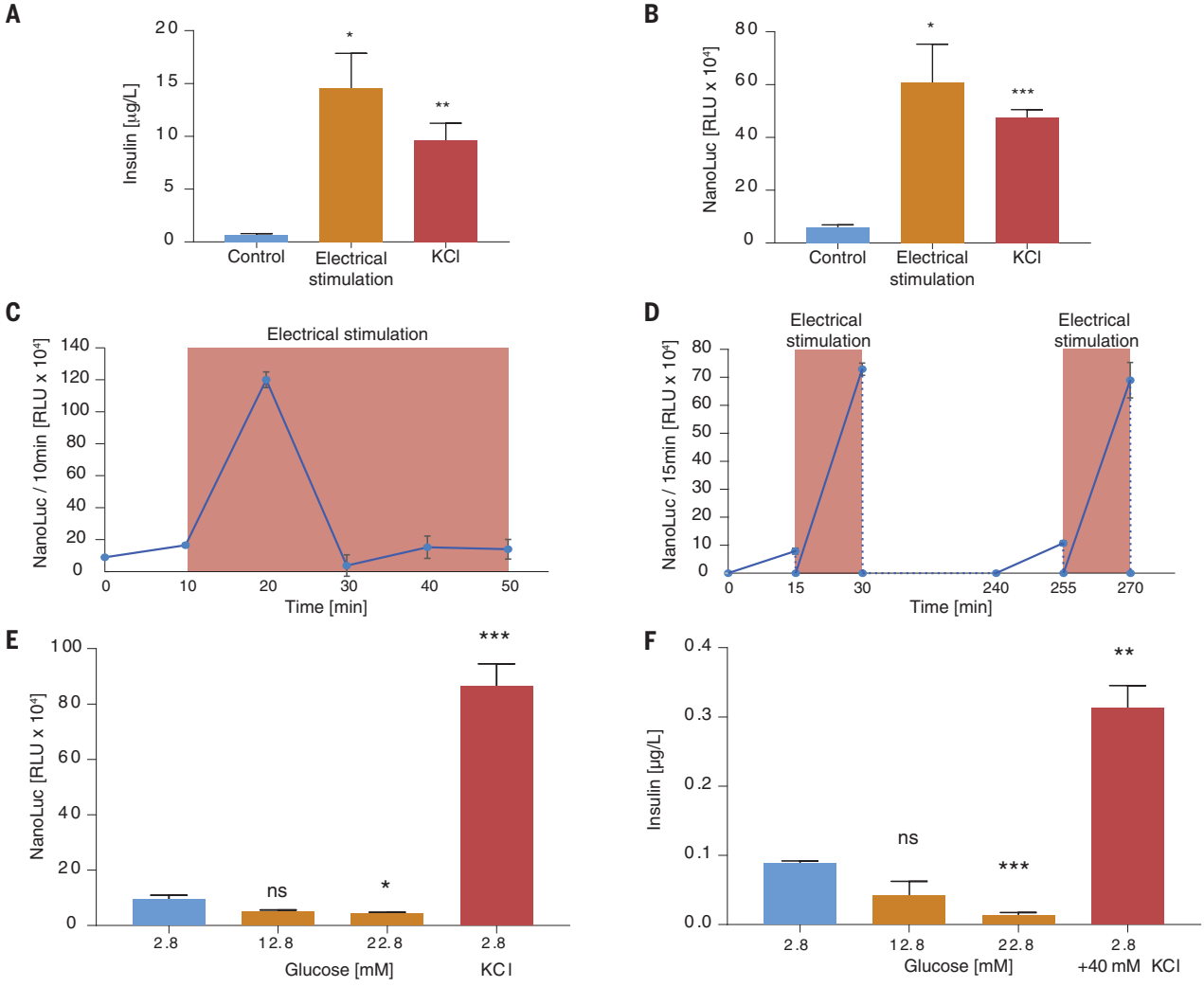

Fig. 6. Functionality of $_{Electro}$β cells in vitro. (**A** and **B**) Electrostimulation of $_{Electro}$β cells. Cells were seeded into cell culture inserts, and 24 hours later they were stimulated with electrical pulses (orange bars) or with 40 mM KCl (red bars). Blue bars denote negative controls. (A) Insulin content in the supernatant from inside the insert (above the cell layer) was measured by ELISA; $n = 3$. (B) Luminescence was measured in supernatant samples taken from inside the insert (above the cell layer); $n = 3$. (**C**) Secretion kinetics. $_{Electro}$β cells were seeded into cell culture inserts and stimulated with electrical pulses (red frame). Luminescence was measured in supernatant samples every 10 min; $n = 4$. (**D**) Reversibility assay. $_{Electro}$β cells were electrostimulated for 15 min twice, with 4-hour time intervals between the first and second electrostimulation; $n = 4$. (**E**) Glucose-induced insulin release. $_{Electro}$β cells were incubated with various concentrations of glucose for 15 min (blue bar, 2.8 mM glucose; orange bars, elevated glucose; red bar, 2.8 mM glucose with 40 mM KCl). Luminescence was measured in supernatant samples; $n = 3$. (**F**) Glucose-induced insulin release. INS_{Vesc} cells were incubated with various concentrations of glucose for 60 min (blue bar, 2.8 mM glucose; orange bars, elevated glucose; red bar, 2.8 mM glucose with 40 mM KCl). Insulin content was quantified in supernatant samples; $n = 3$. Data are means ± SEM. $^*P < 0.05$, $^{**}P < 0.01$, $^{***}P < 0.001$ (versus control).

bioelectronic implant could in principle be powered by batteries (*52*) (table S4), for practical reasons, including the limited space for implantation and the intrusiveness of animal experimentation, we chose to power the device inductively at 13.56 MHz, an FCC-licensed radio frequency that is reserved internationally for industrial, scientific, and medical devices and does not interfere with telecommunications. Because of the power efficiency of the implant, we speculate that wireless-powered control by wearable devices such as smartphones and smartwatches might be feasible in the near future.

However, reaching the full therapeutic potential of electrogenetics will require closed-loop control. Whereas classical medical interventions are open-loop, because the dose is largely determined by the physician on the basis of body weight, closed-loop systems enable feedback control that coordinates biomarker input to therapeutic output and provides an autonomous and self-sufficient interface with patients' metabolism. For electrogenetic type 1 diabetes control, this would mean using electronic blood glucose sensors to directly control electrostimulated insulin release in real time, much like the concepts currently being explored for prototypes of the bionic pancreas (*53*). However, electronic closed-loop systems operating in the bionic pancreas require frequent calibration and have a short lifespan of only a few days (*49*). On the other hand, incorporation of a microcontroller and/or a glucometer into our bioelectronic implant to achieve closed-loop insulin control should be a straightforward electrical engineering implementation. Most important, the delayed resorption of insulin from subcutaneous tissues to which insulin is delivered by the bionic pancreas requires dual-hormone control using glucagon to counteract or prevent

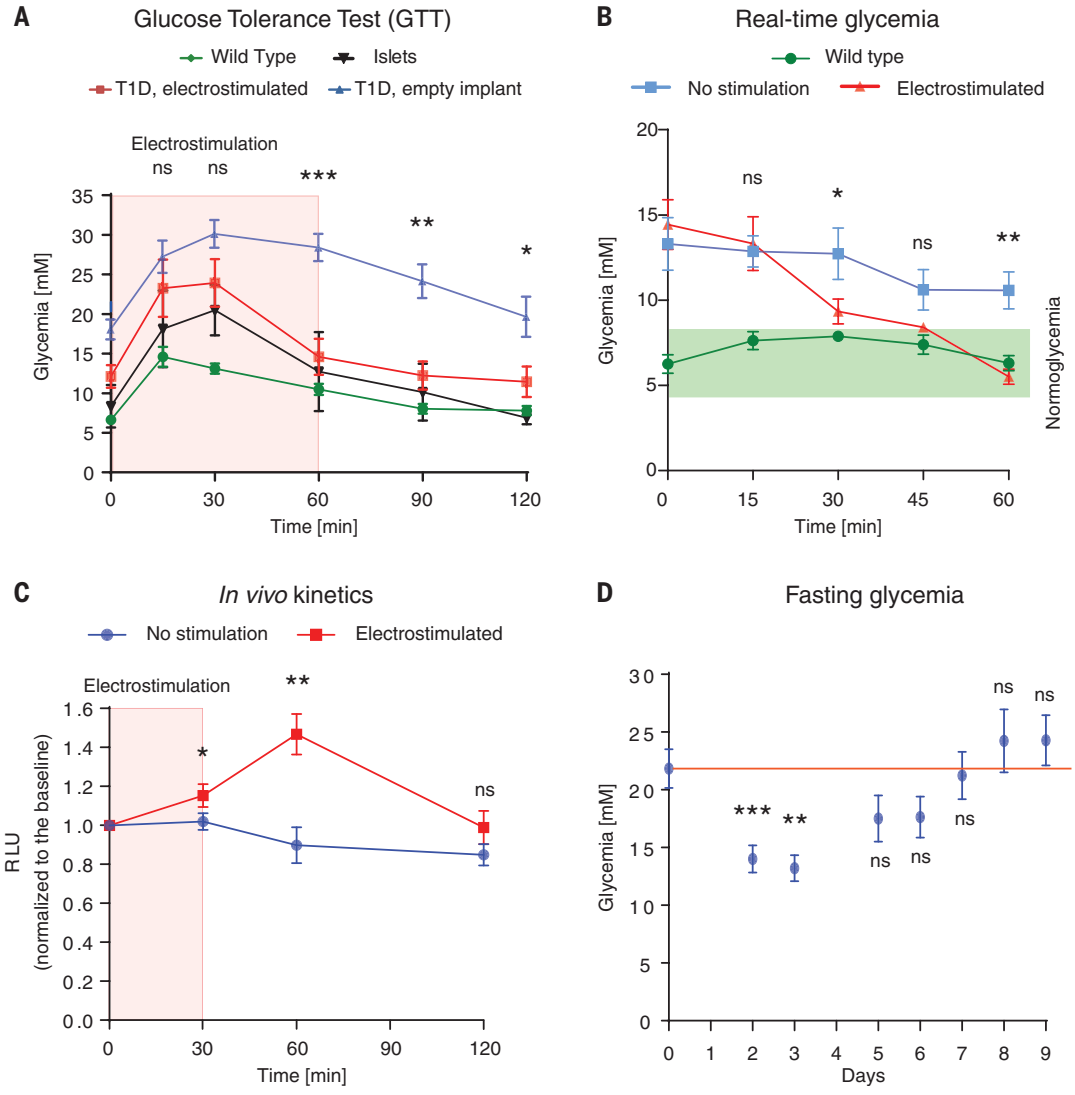

Fig. 7. Comparative analyses of $_{Electro}$β-containing bioelectronic implants in type 1 diabetic mice. Type 1 diabetic mice implanted on the back with $_{Electro}$β-containing bioelectronic devices were profiled for blood glucose dynamics. (**A**) Glucose tolerance test. At 48 hours after implantation, the $_{Electro}$β cells inside the bioelectronic implant were electrostimulated for 60 min (red line), then the animals were given intraperitoneal glucose injections and their blood glucose levels were monitored. All groups received intraperitoneal glucose injection (2 g per kg body weight). Wild type, n = 8; T1D, implant electrostimulated (type 1 diabetes, activated implant), n = 6; T1D, empty implant (type 1 diabetes, implant without cells), n = 10; islets (human pancreatic beta islets), n = 3. Statistical significance of differences between the electrostimulated and mock groups was calculated. (**B**) Real-time glycemia measurement. Fasted type 1 diabetic mice implanted with $_{Electro}$β-containing bioelectronic implants were electrostimulated for 30 min and their glycemic profile was recorded. Nonstimulated control (T1D, implanted mice), n = 6; stimulated group (T1D, implanted mice), n = 7; wild-type controls, n = 6. The green frame indicates the normoglycemic range (4.4 to 7.2 mM). Statistical significance was calculated between electrostimulated mice and nonstimulated controls. (**C**) Blood luciferase kinetics of animals implanted with $_{Electro}$β cell–containing implants electrostimulated for 30 min (red line; n = 6). NanoLuc was quantified from microliter-scale blood samples every 30 min. The blue line indicates the nonelectrostimulated negative control (n = 5); red frame indicates electrostimulation time. Statistical significance of differences versus time point 0 was calculated with a paired t test. (**D**) Fasting glycemia. Type 1 diabetic mice were implanted with $_{Electro}$β-containing bioelectronic implants and fasting glycemia was recorded for more than 1 week. Orange line indicates the initial level of average glycemia. Statistical significance of differences versus time point 0 was calculated with a paired t test. Data are means ± SEM. *P < 0.05, **P < 0.01, ***P < 0.001.

insulin-mediated hypoglycemia (*54*, *55*). We show here that glucagon can be released from pancreatic α cells by vesicular secretion, just as insulin is from β cells; this suggests that a dual-hormone electrogenetic system using two types of engineered cells would be feasible. Nonetheless, dual-hormone control is not expected to be necessary with our electrogenetic system because, as noted above, the dynamics of electrostimulated vesicular insulin secretion from $_{Electro}$β cells appear to be comparable with those of human pancreatic islets. Furthermore, the demonstration that our system works in two different types of cells suggests broad potential applicability of electrogenetics for electrostimulated hormone release in future cell-based therapies.

As in the case of the bionic pancreas (*53*), long-term functionality of cellular implants remains a major challenge in designing next-generation encapsulated cell-based therapeutic devices (*56*). A recent clinical trial using encapsulated pancreatic progenitor cells, the

precursor phenotype of insulin-secreting β cells (ViaCyte's VC-01), confirmed the need for further technological development to promote engraftment (*57*). Long-term functionality of cells inside implants remains among the challenges facing translation of academic proof-of-concept studies into clinical reality. In this context, the first initiatives to improve viability (Beta-O2 Technologies Ltd.; βAir) as well as vascularization of encapsulated cells (*58*) (e.g., ViaCyte's PEC Direct or Sernova's Cell Pouch System) have already begun in industry.

We have shown that wireless electrical stimulation of insulin release by electrosensitive designer cells inside a bioelectronic implant was able to rapidly restore normoglycemia in type 1 diabetic mice. The adoption of wireless electronic devices that can program the release of biopharmaceuticals, either via the secretory pathway or vesicular secretion, by means of direct communication between the device and implanted cells is expected to open up many new opportunities for advanced precision healthcare optimized for individuals.

REFERENCES AND NOTES

1. M. M. Aye, S. L. Atkin, *Drug Healthc. Patient Saf.* **6**, 55–67 (2014).
2. A. Goto, O. A. Arah, M. Goto, Y. Terauchi, M. Noda, *BMJ* **347**, f4533 (2013).
3. G. P. Leese *et al*., *Diabetes Care* **26**, 1176–1180 (2003).
4. C. Uduku, N. Oliver, *Curr. Opin. Pharmacol.* **36**, 29–33 (2017).
5. M. Xie *et al*., *Science* **354**, 1296–1301 (2016).
6. J. Shao *et al*., *Sci. Transl. Med.* **9**, eaal2298 (2017).
7. T. Kushibiki, S. Okawa, T. Hirasawa, M. Ishihara, *Gene Ther.* **22**, 553–559 (2015).
8. T. Kim, M. Folcher, M. Doaud-El Baba, M. Fussenegger, *Angew. Chem. Int. Ed.* **54**, 5933–5938 (2015).
9. H. Ye, M. Daoud-El Baba, R. W. Peng, M. Fussenegger, *Science* **332**, 1565–1568 (2011).
10. M. Folcher *et al*., *Nat. Commun.* **5**, 5392 (2014).
11. H. A. Andersson, Y. S. Kim, B. E. O'Neill, Z. Z. Shi, R. E. Serda, *Vaccines* **2**, 216–227 (2014).
12. V. Ortner *et al*., *J. Control. Release* **158**, 424–432 (2012).
13. H. Huang, S. Delikanli, H. Zeng, D. M. Ferkey, A. Pralle, *Nat. Nanotechnol.* **5**, 602–606 (2010).
14. S. A. Stanley, J. Sauer, R. S. Kane, J. S. Dordick, J. M. Friedman, *Nat. Med.* **21**, 92–98 (2015).
15. M. Fussenegger *et al*., *Nat. Biotechnol.* **18**, 1203–1208 (2000).
16. W. Weber *et al*., *Nat. Biotechnol.* **20**, 901–907 (2002).
17. B. G. Auner, C. Valenta, J. Hadgraft, *J. Control. Release* **89**, 321–328 (2003).
18. M. Gitzinger, C. Kemmer, M. D. El-Baba, W. Weber, M. Fussenegger, *Proc. Natl. Acad. Sci. U.S.A.* **106**, 10638–10643 (2009).
19. M. Gitzinger *et al*., *Nucleic Acids Res.* **40**, e37 (2012).
20. H. Wang, H. Ye, M. Xie, M. Daoud El-Baba, M. Fussenegger, *Nucleic Acids Res.* **43**, e91 (2015).
21. S. A. Stanley *et al*., *Science* **336**, 604–608 (2012).
22. A. Prindle *et al*., *Nature* **508**, 387–391 (2014).
23. W. Weber *et al*., *Nucleic Acids Res.* **37**, e33 (2009).
24. W. Weber *et al*., *Nat. Biotechnol.* **22**, 1440–1444 (2004).
25. T. Tschirhart *et al*., *Nat. Commun.* **8**, 14030 (2017).
26. D. Katz, T. Akiyama, *Ann. Noninvasive Electrocardiol.* **12**, 223–226 (2007).
27. J. H. Stockley *et al*., *Sci. Rep.* **7**, 849 (2017).
28. T. D. Hinds Jr. *et al*., *J. Biol. Chem.* **291**, 25179–25191 (2016).
29. Y. Uda *et al*., *Proc. Natl. Acad. Sci. U.S.A.* **114**, 11962–11967 (2017).
30. Z. Hu *et al*., *Int. J. Mol. Sci.* **16**, 22621–22635 (2015).
31. H. M. Beyer *et al*., *ACS Synth. Biol.* **4**, 951–958 (2015).
32. G. Jarockyte *et al*., *Int. J. Mol. Sci.* **17**, 1193 (2016).
33. B. A. Maher *et al*., *Proc. Natl. Acad. Sci. U.S.A.* **113**, 10797–10801 (2016).
34. F. M. Ashcroft, P. Rorsman, *Nat. Rev. Endocrinol.* **9**, 660–669 (2013).
35. R. Buzzetti, S. Zampetti, E. Maddaloni, *Nat. Rev. Endocrinol.* **13**, 674–686 (2017).
36. D. Jacobs-Tulleneers-Thevissen *et al*., *Diabetologia* **56**, 1605–1614 (2013).
37. T. Desai, L. D. Shea, *Nat. Rev. Drug Discov.* **16**, 338–350 (2017).
38. G. W. Zamponi, J. Striessnig, A. Koschak, A. C. Dolphin, *Pharmacol. Rev.* **67**, 821–870 (2015).
39. M. D'Arco, A. C. Dolphin, *Sci. Signal.* **5**, pe34 (2012).
40. T. Kim *et al*., *Biochem. Biophys. Res. Commun.* **324**, 401–408 (2004).
41. A. Llucià-Valldeperas *et al*., *J. Tissue Eng. Regen. Med.* **9**, E76–E83 (2015).
42. M. H. Thelen, W. S. Simonides, C. van Hardeveld, *Biochem. J.* **321**, 845–848 (1997).
43. Y. Manabe *et al*., *PLOS ONE* **7**, e52592 (2012).
44. J. T. McCluskey *et al*., *J. Biol. Chem.* **286**, 21982–21992 (2011).
45. S. M. Burns *et al*., *Cell Metab.* **21**, 126–137 (2015).
46. J. Gromada, P. Chabosseau, G. A. Rutter, *Nat. Rev. Endocrinol.* **14**, 694–704 (2018).
47. H. Yamashita, D. T. Nguyen, E. Chung, *Methods Mol. Biol.* **1098**, 145–151 (2014).
48. B. Rattner, in *Host Response to Biomaterials*, S. Badylak, Ed. (Academic Press, 2015), pp. 37–51.
49. S. J. Russell *et al*., *Lancet Diabetes Endocrinol.* **4**, 233–243 (2016).
50. P. A. Hollander *et al*., *Diabetes Care* **24**, 983–988 (2001).
51. S. E. Kahn *et al*., *J. Clin. Endocrinol. Metab.* **86**, 5824–5829 (2001).
52. H. G. Mond, G. Freitag, *Pacing Clin. Electrophysiol.* **37**, 1728–1745 (2014).
53. S. J. Russell *et al*., *N. Engl. J. Med.* **371**, 313–325 (2014).
54. G. Schmelzeisen-Redeker *et al*., *J. Diabetes Sci. Technol.* **9**, 1006–1015 (2015).
55. D. B. Keenan, J. J. Mastrototaro, G. Voskanyan, G. M. Steil, *J. Diabetes Sci. Technol.* **3**, 1207–1214 (2009).
56. M. Qi, *Adv. Med.* **2014**, 429710 (2014).
57. R. R. Henry *et al*., *Diabetes* **67** (suppl. 1), 138-OR (2018).
58. Y. Evron *et al*., *Sci. Rep.* **8**, 6508 (2018).

ACKNOWLEDGMENTS

We thank the Geneva Islet Transplantation Center and H. Zulewski for human pancreatic islets, which were obtained through the basic research program of the European Consortium for Islet Transplantation (ECIT). We thank S. Bürgel for help in the initial stage of the project, A. Hierlemann for providing pulse generators, M. Folcher for constructive discussions, E. Siringil for support with 3D printing, B. Lang for advice on statistical analysis, A. M. Palma Teixeira and G. Camenisch for preparation of the animal experimentation applications, A. Graff-Meyer and C. Genoud for taking electron microscopy images, and H. Zhao and N. Franko for their help in assembling implants. **Funding:** Supported by a European Research Council (ERC) advanced grant (ElectroGene; grant no. 785800) and in part by the Swiss National Science Foundation (SNF) National Centre of Competence in Research (NCCR) for Molecular Systems Engineering. ECIT was supported by the Juvenile Diabetes Research Foundation (JDRF; grant 31-2008-416). **Author contributions:** K.K. and M.F. designed the project; K.K. and P.S. performed the cell culture experiments and K.K. designed the implants; K.K., S.X., G.C., M.D.H., J.S., and H.Y. performed the animal experiments; P.B. designed the electronic switchboard; K.K., P.S., M.X., and M.F. designed the experiments and analyzed the results; K.K., P.S., M.X., and M.F. wrote the manuscript; and S.X., M.D.H., M.X., and M.F. designed the modified implants and the in vivo "refill" as well as the insulin kinetics experiments. **Competing interests:** The authors declare no competing financial interests. **Data and materials availability:** The authors declare that all the data supporting the findings of this study are available within the paper and its supplementary materials. Original plasmids are available upon request. All vector information is provided in table S7.

SUPPLEMENTARY MATERIALS

science.sciencemag.org/content/368/6494/993/suppl/DC1
Materials and Methods
Figs. S1 to S20
Tables S1 to S8
References (*59*–*69*)

9 July 2018; resubmitted 11 February 2020
Accepted 3 April 2020
10.1126/science.aau7187

Electrogenetic cellular insulin release for real-time glycemic control in type 1 diabetic mice

Krzysztof Krawczyk, Shuai Xue, Peter Buchmann, Ghislaine Charpin-El-Hamri, Pratik Saxena, Marie-Didie Hussherr, Jiawei Shao, Haifeng Ye, Mingqi Xie, and Martin Fussenegger

Science, **368** (6494), .
DOI: 10.1126/science.aau7187

Electronic control of designer cells

There is increasing interest in using designer cells to produce or deliver therapeutics. Achieving direct communication between such cells and electronic devices would allow precise control of therapies. Krawczyk *et al.* describe a bioelectronic interface that uses wireless-powered electrical stimulation of cells to promote the release of insulin (see the Perspective by Brier and Dordick). The authors engineered human # cells to respond to membrane depolarization by rapidly releasing insulin from intracellular storage vesicles. A bioelectronic device that incorporates the cells can be wirelessly triggered by an external field generator. When subcutaneously implanted in type 1 diabetic mice, the device could be triggered to restore normal blood glucose levels.

Science, this issue p. 993; see also p. 936